Eur. Phys. J. C (2023) 83:725
https://doi.org/10.1140/epjc/s10052-023-11884-2

THE EUROPEAN PHYSICAL JOURNAL C

Regular Article - Theoretical Physics

The Z resonance, inelastic dark matter, and new physics anomalies in the Simple Extension of the Standard Model (SESM) with general scalar potential

Wenxing Zhang[1,a], **Tianjun Li**[2,3,b], **Xiangwei Yin**[2,3,c]

[1] Tsung-Dao Lee Institute and School of Physics and Astronomy, Shanghai Jiao Tong University, 800 Dongchuan Rd., Minhang, Shanghai 200240, China
[2] CAS Key Laboratory of Theoretical Physics, Institute of Theoretical Physics, Chinese Academy of Sciences, Beijing 100190, China
[3] School of Physical Sciences, University of Chinese Academy of Sciences, No. 19A Yuquan Road, Beijing 100049, China

Received: 1 April 2023 / Accepted: 30 July 2023 / Published online: 13 August 2023

Abstract We consider the generic scalar potential with CP-violation, and study the Z resonance and inelastic dark matter in the Simple Extension of the Standard Model (SESM), which can explain the dark matter as well as new physics anomalies such as the B physics anomalies and muon anomalous magnetic moment, etc. With the new scalar potential terms, we obtain the mass splittings for the real and imaginary parts of scalar fields. And thus we can have the DM co-annihilation process mediated by Z boson, which couples exclusively to the CP-even and CP-odd parts of scalar fields. This is a brand new feature compared to the previous study. For the CP conserving case, we present the viable parameter space for the Higgs and Z resonances, which can explain the B physics anomalies, muon anomalous magnetic moment, and dark matter relic density, as well as evade the constraint from the XENON1T direct detection simultaneously. For the CP-violating case, we consider the inelastic dark matter, and study four concrete scenarios for the inelastic DM-nucleon scatterings mediated by the Higgs and Z bosons in details. Also, we present the benchmark points which satisfy the aforementioned constraints. Furthermore, we investigate the constraints from the dark matter-electron inelastic scattering processes mediated by the Higgs and Z bosons in light of the XENONnT data. We show that the constraint on the Z mediated process is weak, while the Higgs mediated process excludes the dark matter with mass around several MeV.

[a] e-mail: zhangwenxing@sjtu.edu.cn
[b] e-mail: tli@itp.ac.cn
[c] e-mail: yinxiangwei@itp.ac.cn (corresponding author)

1 Introduction

The celebrated theory known as the Standard Model (SM) of particle physics has been confirmed to be an effective description of our nature at the low energy scale after the discovery of Higgs boson at the LHC in 2012 [1,2]. However, some inconsistence phenomena are much discomforting, for instance, dark matter (DM), dark energy, neutrino masses and mixings, and matter–antimatter asymmetry, etc. Besides, there exist a few big fine-tuning problems, for example, cosmological constant problem, gauge hierarchy problem, and strong CP problem, etc. Thus, we need to explore the new physics beyond the SM.

One of the pressing extensions is in flavour sector. The LHCb Collaboration has observed the persistent discrepancies between the SM predictions and experimental measurements for rare decays of B mesons in several years, for example, the angular distribution of $B \to K\mu^+\mu^-$ and Lepton Flavor Universality (LFU) ratios $R_K = BR(B \to \mu\mu)/BR(B \to ee)$ [3–11]. The recent measurements of $B^+ \to K^+\ell^+\ell^-$ and $B^0 \to K^{*0}\ell^+\ell^-$ decays have been presented to test the muon-electron universality in two ranges of the square of the dilepton invariant mass [12,13]. The results seems compatible with the SM predictions. However, this is not the final result, since this is just one measurement with the limited precision. In fact, the data used in such analyses are only few percents of LHC data. In addition, although the misidentification backgrounds for electron channel were underestimated in the previous measurement of R_K/R_{K^*}, the measurements for the muon channels are still correct. Also, for the $b \to s\mu^+\mu^-$ differential decay branching ratio, there still exist the theoretical and experimental deviations in the low q^2 region, and P_5', etc. Thus,

the B physics anomalies are still worth considering. The measurements of the anomalous magnetic moment of muon, $a_\mu = (g-2)_\mu/2$, is one of the most important directions to probe new physics (NP). The state-of-the-art measurements declared by the Fermilab experiment shows 4.2 σ discrepancy between the SM prediction and experimental value [14]. This makes muon g-2 an intriguing topic in the future [15–23]. Moreover, there exist compelling evidences for the DM existence from both particle physics and astronomy. However, there exists a wide range of mass for the DM candidates, making DM physics a fruitful theme. for a review, see [24]. Furthermore, The XENON1T experiment has found a low-energy electron recoil signal about $1 \sim 7$ keV [25]. But the signal was excluded by the XENONnT experiment [26], setting new constraints on various models.

In this paper, we consider the general scalar potential with CP-violation and the inelastic dark matter in the Simple Extension of the Standard Model (SESM) [27,28]. In this model, we can address R_K, $B_s - \bar{B}_s$ oscillation, muon anomalous magnetic moment, dark matter, and evade the XENON1T direct detection simultaneously, etc. With the new scalar potential terms, we obtain the mass splittings for the real and imaginary parts of scalar fields. And thus we can have the DM co-annihilation process mediated by Z boson, which couples exclusively to the CP-even and CP-odd parts of scalar fields. This is a brand new feature compared to the Ref. [28]. For the CP conserving case, we present the viable parameter space for the Higgs and Z resonances, which can explain the B physics anomalies, muon g-2, and DM relic density, as well as evade the constraint from the XENON1T direct detection simultaneously. For the CP-violating case, we discuss the inelastic dark matter, and consider four concrete scenarios for the inelastic DM-nucleon scatterings mediated by the Higgs and Z bosons in details. Also, we present the benchmark points which satisfy the aforementioned constraints. Furthermore, we investigate the constraints from the dark matter-electron inelastic scattering processes mediated by the Higgs and Z bosons in light of the XENONnT data. We show that the constraint on the Z mediated process is weak, while the Higgs mediated process excludes the dark matter with mass around several MeV.

This paper is organized as follows. In Sect. 2, we introduce the SESM, and discuss the scalar masses. In Sect. 3, we address the new physics anomalies and DM as mentioned above. In Sect. 4, four types of inelastic DM scenarios are discussed. In Sect. 5, the constraints to our model by considering the null excess signals of XENONnT data are studied. We conclude in Sect. 6.

2 The Simple Extension of the Standard Model (SESM)

The SESM [27,28] has been proposed to address the tentative new physics anomalies and DM in its own right. The model introduces a singlet complex scalar Φ_S, a doublet complex scalar Φ_D, a vector like quark Q', and a vectorlike lepton L'. All these exotic fields are odd under a discrete Z_2 symmetry while the SM field are even. The quantum numbers of additional fields are

Field	spin	$SU(3)_C$	$SU(2)_L$	$U(1)_Y$
Q'	1/2	**3**	**2**	1/6
L'	1/2	**1**	**2**	−1/2
Φ_S	0	**1**	**1**	0
Φ_D	0	**1**	**2**	−1/2

(1)

The new fields can be written as

$$Q' = \begin{pmatrix} U' \\ D' \end{pmatrix}, \quad L' = \begin{pmatrix} L'^0 \\ L'^- \end{pmatrix},$$
$$\Phi_S \equiv S_s^0, \quad \Phi_D = \begin{pmatrix} S_d^0 \\ S^- \end{pmatrix}. \tag{2}$$

The Lagrangian is given by

$$\begin{aligned}
\mathcal{L} \supset & \left(\lambda_i^Q \overline{Q'} Q_i \Phi_S + \lambda_i^U \overline{Q'} U_i \Phi_D + \lambda_i^D \overline{Q'} D_i \widetilde{\Phi}_D \right. \\
& + \lambda_i^L \overline{L'} L_i \Phi_S + \lambda_i^E \overline{L'} E_i \widetilde{\Phi}_D + a_H H^\dagger \widetilde{\Phi}_D \Phi_S \\
& \left. + a'_H H^\dagger \widetilde{\Phi}_D \Phi_S^\dagger + \lambda''_{DH} \left(\widetilde{\Phi}_D^\dagger H \right)^2 + \lambda'_{SH} \Phi_S^2 |H|^2 + \text{h.c.} \right) \\
& - M_Q \overline{Q'} Q' - M_L \overline{L'} L' - M_S^2 |\Phi_S|^2 \\
& + M_S'^2 \left(\Phi_S^2 + \Phi_S^{\star 2} \right) - M_D^2 |\Phi_D|^2 - M_H^2 |H|^2 \\
& + \frac{\lambda_S}{2} \left(\Phi_S^+ \Phi_S \right)^2 + \lambda'_S \left(\Phi_S^2 + \Phi_S^{\star 2} \right) |\Phi_S|^2 \\
& + \lambda''_S \left(\Phi_S^4 + \Phi_S^{\star 4} \right) + \frac{\lambda_D}{2} \left(\Phi_D^+ \Phi_D \right)^2 + \frac{\lambda_H}{2} |H|^4 \\
& + \lambda_{SD} |\Phi_S|^2 |\Phi_D|^2 + \lambda'_{SD} \left(\Phi_S^2 + \Phi_S^{\star 2} \right) |\Phi_D|^2 \\
& + \lambda_{SH} |\Phi_S|^2 |H|^2 + \lambda_{DH} |\Phi_D|^2 |H|^2 \\
& + \lambda'_{DH} \left(H^\dagger \widetilde{\Phi}_D \right) \left(\widetilde{\Phi}_D^\dagger H \right),
\end{aligned} \tag{3}$$

where H is the SM Higgs field, and we denote the left-handed quark doublets, right-handed up-type quarks, right-handed down-type quarks, left-handed lepton doublets, and right-handed down-type leptons as Q_i, U_i, D_i, L_i, and E_i ($i = 1, 2, 3$), respectively.

After the electroweak symmetry breaking (EWSB), the above λ_{SH} and λ'_{SH} terms will contribute to the mass of Φ_S, while the λ_{DH}, λ'_{DH}, and λ''_{DH} terms will contribute to the mass of Φ_D. Especially, we have the real and imaginary parts splittings of new scalars due to the a_H, a'_H $M_S'^2$, λ'_{SH} and λ''_{DH} terms. In the next Section, we can obtain the inelastic DM co-annihilations through the Z resonance because of such splittings.

Assume that CP is conserved, we obtain the mass square matrix of the real parts of Φ_S and Φ_D

$$\begin{pmatrix} M_S{}^2 - 2M_S'{}^2 + \frac{v^2\lambda_{SH}}{2} - v^2\lambda'_{SH} & \frac{(a'_H - a_H)v}{\sqrt{2}} \\ \frac{(a'_H - a_H)v}{\sqrt{2}} & M_D^2 + \frac{v^2\lambda_{DH}}{2} - \frac{v^2\lambda'_{DH}}{2} - v^2\lambda''_{DH} \end{pmatrix}, \tag{4}$$

and the mass square matrix of their imaginary parts is

$$\begin{pmatrix} M_S{}^2 + 2M_S'{}^2 + \frac{v^2\lambda_{SH}}{2} + v^2\lambda'_{SH} & \frac{(a_H + a'_H)v}{\sqrt{2}} \\ \frac{(a_H + a'_H)v}{\sqrt{2}} & M_D^2 + \frac{v^2\lambda_{DH}}{2} - \frac{v^2\lambda'_{DH}}{2} + v^2\lambda''_{DH} \end{pmatrix}, \tag{5}$$

where $v \simeq 246$ GeV is the vacuum expectation value of the Higgs field. And the corresponding mass eigenvalues of real parts are

$$\begin{aligned} M_{S_1}{}^2 &= \frac{1}{4}\Big(2M_D^2 + 2M_S^2 - 4M_S'{}^2 + v^2\left(\lambda_{DH}\right. \\ &\quad \left. -\lambda'_{DH} - 2\lambda''_{DH} + \lambda_{SH} - 2\lambda'_{SH}\right) - \sqrt{A+B}\Big), \\ M_{S_2}{}^2 &= \frac{1}{4}\Big(2M_D^2 + 2M_S^2 - 4M_S'{}^2 + v^2\left(\lambda_{DH}\right. \\ &\quad \left. -\lambda'_{DH} - 2\lambda''_{DH} + \lambda_{SH} - 2\lambda'_{SH}\right) + \sqrt{A+B}\Big), \end{aligned} \tag{6}$$

where A and B are defined as

$$\begin{aligned} A &= 4\left(M_D^2 - M_S^2 + 2M_S'{}^2\right)^2 + 8(a_H - a'_H)^2 v^2, \\ B &= v^2\left(\lambda_{DH} - \lambda'_{DH} - 2\lambda''_{DH} - \lambda_{SH} + 2\lambda'_{SH}\right) \\ &\quad \times \Big(4\left(M_D^2 - M_S^2 + 2M_S'{}^2\right) \\ &\quad + v^2\left(\lambda_{DH} - \lambda'_{DH} - 2\lambda''_{DH} - \lambda_{SH} + 2\lambda'_{SH}\right)\Big). \end{aligned}$$

The corresponding mass eigenvalues of imaginary parts are

$$\begin{aligned} M_{S_1'}^2 &= \frac{1}{4}\Big(2M_D^2 + 2M_S^2 + 4M_S'{}^2 + v^2\left(\lambda_{DH}\right. \\ &\quad \left. -\lambda'_{DH} + 2\lambda''_{DH} + \lambda_{SH} + 2\lambda'_{SH}\right) - \sqrt{C+D}\Big), \\ M_{S_2'}^2 &= \frac{1}{4}\Big(2M_D^2 + 2M_S^2 + 4M_S'{}^2 + v^2\left(\lambda_{DH}\right. \\ &\quad \left. -\lambda'_{DH} + 2\lambda''_{DH} + \lambda_{SH} + 2\lambda'_{SH}\right) + \sqrt{C+D}\Big), \end{aligned} \tag{7}$$

where C and D are defined as

$$\begin{aligned} C &= 4\left(M_S^2 - M_D^2 + 2M_S'{}^2\right)^2 + 8(a_H + a'_H)^2 v^2, \\ D &= v^2\left(\lambda_{DH} - \lambda'_{DH} + 2\lambda''_{DH} - \lambda_{SH} - 2\lambda'_{SH}\right) \\ &\quad \times \Big(4\left(M_D^2 - M_S^2 - 2M_S'{}^2\right) \\ &\quad + v^2\left(\lambda_{DH} - \lambda'_{DH} + 2\lambda''_{DH} - \lambda_{SH} - 2\lambda'_{SH}\right)\Big). \end{aligned}$$

In addition, the couplings between the vectorlike quark Q' and the up/down-type quarks are the same as [27,28]. And the lightest real or imaginary part of the scalars is the DM candidate.

3 Flavour observables and dark matter

In the SESM, besides the two charged scalar particles, there are four neutral scalar particles, the real (imaginary) parts of scalar fields $S_1(S_1')$ and $S_2(S_2')$. In the following, we consider either S_1 or S_1' be the DM candidate and assume the mass difference between S_1 and S_1' is less than several GeVs, and then they can be regarded as approximately degenerate.

3.1 R_K and B_s mixing

The effective operators contributing to R_K are [27]

$$\begin{aligned} \mathcal{H}_{\text{eff}}^{bs\mu\mu} \supset -\mathcal{N}\Big[& C_9^{bs\mu\mu}\left(\bar{s}\gamma_\mu P_L b\right)\left(\bar{\mu}\gamma^\mu \mu\right) \\ & + C_{10}^{bs\mu\mu}\left(\bar{s}\gamma_\mu P_L b\right)\left(\bar{\mu}\gamma^\mu\gamma_5 \mu\right) + \text{ h.c.}\Big], \end{aligned} \tag{8}$$

with the normalization factor

$$\mathcal{N} \equiv \frac{4G_F}{\sqrt{2}}\frac{e^2}{16\pi^2}V_{tb}V_{ts}^*. \tag{9}$$

The contributions to $C_{9,10}^{bs\mu\mu}$ induced by the exotic particles can be written as

$$\begin{aligned} \Delta C_9^{bs\mu\mu} &= -\frac{\lambda_3^{Q_d}\lambda_2^{Q_d *}}{128\pi^2\mathcal{N}}\sum_{\alpha=1,2}\frac{|U_{1\alpha}|^4\left|\lambda_2^L\right|^2 + |U_{1\alpha}|^2|U_{2\alpha}|^2\left|\lambda_2^E\right|^2}{M_{S_\alpha}^2} \\ &\quad \times F_2\left(\frac{M_Q^2}{M_{S_\alpha}^2}, \frac{M_L^2}{M_{S_\alpha}^2}\right), \end{aligned} \tag{10}$$

$$\begin{aligned} \Delta C_{10}^{bs\mu\mu} &= \frac{\lambda_3^{Q_d}\lambda_2^{Q_d *}}{128\pi^2\mathcal{N}}\sum_{\alpha=1,2}\frac{|U_{1\alpha}|^4\left|\lambda_2^L\right|^2 - |U_{1\alpha}|^2|U_{2\alpha}|^2\left|\lambda_2^E\right|^2}{M_{S_\alpha}^2} \\ &\quad \times F_2\left(\frac{M_Q^2}{M_{S_\alpha}^2}, \frac{M_L^2}{M_{S_\alpha}^2}\right), \end{aligned} \tag{11}$$

with the loop function

$$F_2(x,y) \equiv \frac{1}{(x-1)(y-1)} + \frac{x^2 \log x}{(x-1)^2(x-y)} + \frac{y^2 \log y}{(y-1)^2(y-x)}. \quad (12)$$

According to the up-to-date fitting [4] ($2\,\sigma$), $\Delta C_9^{bs\mu\mu}$ and $\Delta C_{10}^{bs\mu\mu}$ need to satisfy

$$6.74 + 9.04(\Delta C_9^{bs\mu\mu})^2 + \Delta C_9^{bs\mu\mu}(14.96 - 10.68\Delta C_{10}^{bs\mu\mu}) + \Delta C_{10}^{bs\mu\mu}(-13.22 + 11.90\Delta C_{10}^{bs\mu\mu}) \leq 1. \quad (13)$$

The effective operators contributing to the $B_s - \bar{B}_s$ oscillations are

$$\mathcal{H}_{\text{eff}}^{bd_i} \supset C_1^{bd_i} \left(\overline{d_i}\gamma_\mu P_L b\right)\left(\overline{d_i}\gamma^\mu P_L b\right) + \text{ h.c.} \quad d_i = d, s. \quad (14)$$

The $Q' - \Phi_S$ box diagram gives Wilson coefficients

$$\Delta C_1^{bd_i} = \frac{\left(\lambda_3^{Q_d}\lambda_i^{Q_d *}\right)^2}{128\pi^2} \sum_{\alpha=1,2} \frac{|U_{1\alpha}|^4}{M_{S_\alpha}^2} F\left(\frac{M_Q^2}{M_{S_\alpha}^2}\right), \quad (15)$$

with the loop function

$$F(x) \equiv \frac{x^2 - 1 - 2x\log x}{(x-1)^3}. \quad (16)$$

The latest bound [33,34] is

$$\Delta C_1^{bs} < 2.1 \times 10^{-5}\,\text{TeV}^{-2}. \quad (17)$$

3.2 Muon anomalous magnetic moment

The chirally-enhanced contribution induced by exotic particles to a_μ is

$$\Delta a_\mu \approx -\frac{m_\mu M_L}{8\pi^2} \sum_{\alpha=1,2} \frac{\text{Re}\left(\lambda_2^L \lambda_2^{E*} U_{1\alpha} U_{2\alpha}^*\right)}{M_{S\alpha}^2} f_{LR}\left(\frac{M_L^2}{M_{S_\alpha}^2}\right), \quad (18)$$

where the loop function is

$$f_{LR}(x) \equiv \frac{3 - 4x + x^2 + 2\log x}{2(x-1)^3}. \quad (19)$$

The latest (1σ) discrepancy is given by [14]

$$a_\mu^{\text{EXP}} - a_\mu^{\text{SM}} = (2.51 \pm 0.59) \times 10^{-9}. \quad (20)$$

3.3 Dark matter

With the mass splittings between the real and imaginary parts of new scalar fields, the DM co-annihilation process via Z boson appears. In this section, we mainly consider the Z pole, and thus impose the following three conditions for it. First, because the Z boson couples exclusively to the CP-even and CP-odd components of S_s^0 and S_d^0, we should have the mass splitting between the real and imaginary parts which can be induced by the a_H, a'_H M'^2_S, λ'_{SH} and λ''_{DH} terms in Eq. (3). Second, the mass difference between the real and imaginary parts must be small in order to realize the co-annihilation process. Third, the doublet component of the DM should be considerable.

In Fig. 1, we illustrate the points satisfied the constraints of R_K ($2\,\sigma$) and $B_s - \bar{B}_s$ (black points), the muon g-2 ($1\,\sigma$, blue points), DM relic density (red points) and XENON1T direct detection (green points). We can obtain the correct dark matter relice density via the Higgs mediated DM annihilation as before, and we do not need to consider the inelastic dark matter in this case. Interestingly, we can also obtain the correct dark matter relice density via the Z mediated co-annihilation, which is a new feature compared to Ref. [28]. We need to point out that the direct detection is so strict in the small mass regions that the cross section should be rescaled, thus the direct detection favors the undersaturated DM abundance. The corresponding DM (co-)annihilation processes are demonstrated in Fig. 2, and the benchmark points (some of the green points in Fig. 1) are displayed in Table 1. Point 1 and Point 2 correspond to the Z-mediated DM co-annihilation processes, Point 3 and Point 4 correspond to the Higgs-mediated DM annihilation processes. All these points satisfied the constraints of R_K, $B_s - \bar{B}_s$, muon g-2, DM relic density, and XENON1T direct detection simultaneously.

Finally, we would like to comment about the electroweak precision. Since first we impose the Z_2 symmetry in the model, where SM particles are Z_2 even and the new particles are Z_2 odd. Second, the mass splittings between charged parts and neutral parts of scalar and new fermions are assumed to be zero, thus there is no limitation to electroweak precision tests.

4 The CP violation and inelastic dark matter

In this section, we shall consider the CP-violation and inelastic dark matter. The CP-violation can be realized in our model by considering the complex couplings of a_H, a'_H, and λ'_{SH} in Eq. 3. The modified mass matrix is given by

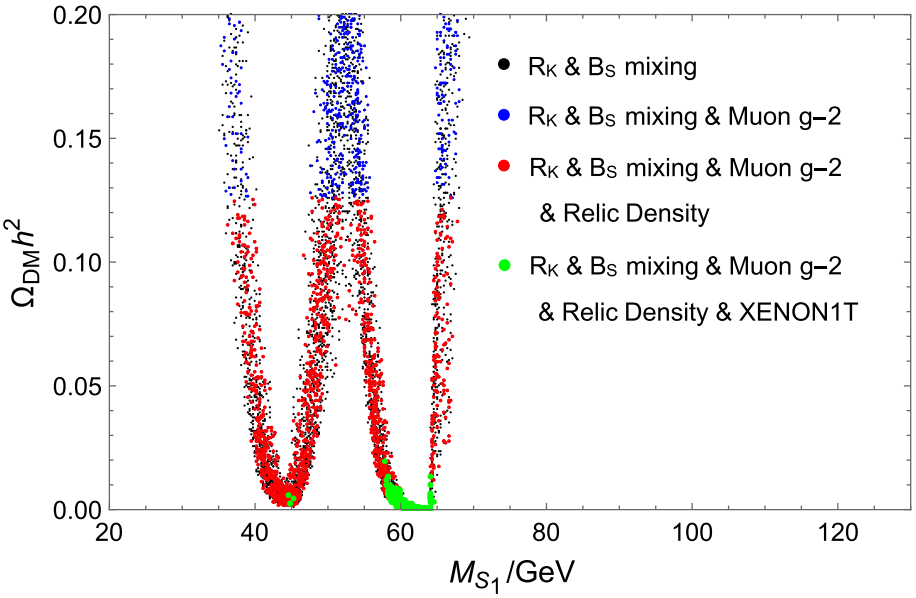

Fig. 1 DM (co-)annihilation mediated by Z and Higgs resonances. The black, blue, red, and green dots satisfy the constraints of R_K ($2\,\sigma$) and $B_s - \bar{B}_s$, muon g-2 ($1\,\sigma$), DM relic density, and XENON1T direct detection in order

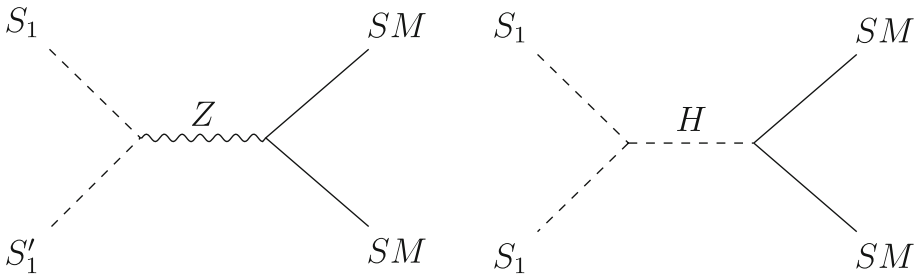

Fig. 2 The DM (co-)annihilation process

$$\begin{pmatrix} M_S{}^2 + 2M_S'{}^2 + \frac{v^2\lambda_{SH}}{2} + v^2 Re(\lambda'_{SH}) & -Im(\lambda'_{SH})v^2 & \frac{(Re(a'_H)+Re(a_H))v}{\sqrt{2}} & \frac{(Im(a_H)+Im(a'_H))v}{\sqrt{2}} \\ -Im(\lambda'_{SH})v^2 & M_S{}^2 - 2M_S'{}^2 + \frac{v^2\lambda_{SH}}{2} - v^2 Re(\lambda'_{SH}) & \frac{(Im(a_H)-Im(a'_H))v}{\sqrt{2}} & \frac{(Re(a'_H)-Re(a_H))v}{\sqrt{2}} \\ \frac{(Re(a'_H)+Re(a_H))v}{\sqrt{2}} & \frac{(Im(a_H)-Im(a'_H))v}{\sqrt{2}} & M_D^2 + \frac{v^2\lambda_{DH}}{2} - \frac{v^2\lambda'_{DH}}{2} + v^2\lambda''_{DH} & 0 \\ \frac{(Im(a_H)+Im(a'_H))v}{\sqrt{2}} & \frac{(Re(a'_H)-Re(a_H))v}{\sqrt{2}} & 0 & M_D^2 + \frac{v^2\lambda_{DH}}{2} - \frac{v^2\lambda'_{DH}}{2} - v^2\lambda''_{DH} \end{pmatrix}. \tag{21}$$

From Eq. 21, we obtain the mass matrices in Eqs. 4 and 5 when we turn off the imaginary parts of a_H, a'_H, and λ'_{SH}. The general interactions between the new scalars and SM Higgs field are given in Eq. A3, which corresponds to scenario III. In scenario I, II, and IV, we have two block diagonal mass matrixes since the absence of imaginary parts of coupling constants. Then the interactions can be reduced to Eqs. A1, A2 and A4. The mass eigenstate are numerically calculated in the following discussions.

These complex couplings can induce the inelastic DM scattering processes, and the $S_1 S_1' h$ coupling arises due to the CP-violation interaction between exotic scalar fields and SM Higgs boson. In this Section, we investigate four kinds of inelastic DM scenarios and there exist the viable parameter space in our model. For simplicity, we give the benchmark points which are consistent with R_K, $B_s - \bar{B}_s$, muon g-2, Xenon1T direct detection, and DM relic density simultaneously. Moreover, the Higgs mediated inelastic processes cansaturate the DM relic density while Z mediated one is undersaturated due to the smaller scalar mass splitting.

4.1 Scenario I: Higgs mediated $S_1 N \to S_2 N'$

The Higgs mediated inelastic DM-nucleon scattering process is shown in Fig. 3a, where S_1 and S_2 are the real parts of scalar fields, N and N' are nucleons before and after scattering. To achieve this kind of scenario, we need to suppress the couplings like $S_1 S_1 h$, $S_1 S_1' h$, and $S_1 S_2' h$, etc.

Table 1 The benchmark points for the DM annihilation and co-annihilation. All the points are consistent with R_K, $B_s - \bar{B}_s$, muon g-2, Xenon1T direct detection, and DM relic density simultaneously

	Point 1	Point 2	Point 3	Point 4
Relic density	0.002324	0.004407	0.000056	0.000103
M_{S_1}/GeV	44.9020863	45.1852846	62.6676439	62.8656877
M_{S_2}/GeV	105.757632	105.721226	117.245807	129.928019
$M_{S_1'}$/GeV	44.568636	44.8051653	63.3885604	62.9503338
$M_{S_2'}$/GeV	105.879782	105.816872	116.41058	129.869903
a_H/GeV	− 16.5052592	− 14.3744695	− 19.73936	− 18.3329214
a'_H/GeV	0.13992708	0.0582310513	0.57179383	0.0376930898
M_S/GeV	54.9009796	52.3632109	73.3372329	69.3362989
M'_S/GeV	0.528484022	1.9419098	2.52399856	3.61952121
M_D/GeV	101.033086	101.974629	110.642889	126.70021
$M_{L'}$/GeV	729.517764	742.893444	854.330313	942.259851
$M_{Q'}$/GeV	3902.10638	3937.67224	3925.43003	3904.98369
λ_{SH}	− 0.000133829454	0.000882003049	0.000915186305	− 0.000205331286
λ'_{SH}	− 0.000641529771	− 0.000559134158	− 0.00062157876	− 0.000389952102
λ_{DH}	− 0.000593605144	0.000790845034	− 0.000583304638	− 0.0000846866652
λ'_{DH}	0.0000286857473	− 0.000668477037	0.000283245864	0.000676767623
λ''_{DH}	0.000599468449	0.000319470619	− 0.000448653707	− 0.0000789446352
λ_2^Q	− 0.477980508	− 0.419005841	− 0.441268492	− 0.437252366
λ_3^Q	0.842752986	0.859113671	0.756431246	0.837793862
λ_2^L	2.23637283	2.47117928	2.48490618	2.22319786
λ_2^E	0.00183980931	0.00243037424	0.00156155801	0.00260726908
$\lambda_S/2$	− 0.129885309	− 0.186246721	− 0.190968994	− 0.248878009
$\lambda'_S/2$	− 0.763678112	− 0.674083096	− 0.893186053	− 0.760477119
$\lambda''_S/2$	− 0.688219001	− 0.522936927	− 0.581113359	− 0.516623688
$\lambda_D/2$	− 0.652102746	− 0.797238171	− 0.626557022	− 0.787219103
λ_{SD}	1.7597484	1.71116141	1.83634899	1.70180638
λ'_{SD}	0.862490095	0.741513741	0.702268647	0.861440253

In Table 2, we elaborate a concrete realization of scenario I, and the corresponding benchmark point is Point 1 in Table 5, where all the points are consistent with R_K, $B_s - \bar{B}_s$, muon g-2, Xenon1T direct detection, and DM relic density simultaneously. We denote the red marks as the most efficient vertex to realize the corresponding scenario, as well as employ the blue and green marks as the vertexes which are forbidden by the mixing angle and mass splitting, respectively. For instance, we choose $\lambda''_{DH} = 0.05$, $\lambda_{DH} = 0.2$, $\lambda'_{DH} = 0.1$, $Re(a_H) = -Re(a'_H) = 0.138149275$, and $\lambda_{SH} = Re(\lambda'_{SH}) = Im(\lambda'_{SH}) = Im(a_H) = Im(a'_H) = 0$. One can check that the opposite sign between a_H and a'_H eliminates the mixing of imaginary parts of the singlet and doublet scalars, which means $U'_{12} = U'_{21} = 0$, and thus explains the origin of the blue marks in Table 2. The $S_1 S_2 h$ vertex marked as red is enhanced by the mixing angle of the real parts of the singlet and doublet scalars, and is responsible for efficiently realizing this kind of scenario. All the remaining vertexes exactly vanish by a comprehensive consideration of the parameters we take above.

4.2 Scenario II: Higgs mediated $S'_1 N \to S'_2 N'$

As shown in Fig. 3b, we come to the second scenario, in which the DM candidate is the imaginary part of scalar field. The concrete realization is presented in Table 3, and the benchmark point is Point 2 in Table 5. Similar to scenario I, the same sign between a_H and a'_H eliminates the mixing of real parts of the singlet and doublet scalars, which means $U_{12} = U_{21} = 0$. The corresponding vertexes are marked as blue, and the red mark is the most efficient vertex to realize scenario II.

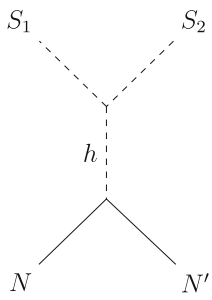

(a) Higgs mediated DM-nucleon scattering.

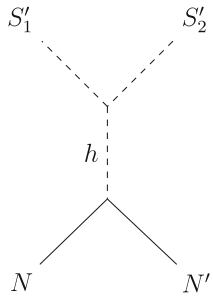

(b) Higgs mediated DM-nucleon scattering.

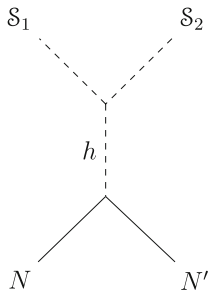

(c) Higgs mediated DM-nucleon scattering.

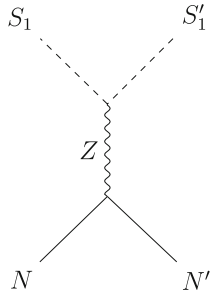

(d) Z mediated DM-nucleon scattering.

Fig. 3 The inelastic DM-nucleon scattering processes

Table 2 The couplings in scenario I

	couplings	S_1S_1h	$S_1S_1'h$	S_1S_2h	$S_1S_2'h$	$S_1'S_1'h$	$S_1'S_2'h$
S_iS_jh	$(2\lambda''_{DH}-\lambda_{DH}+\lambda'_{DH})U_{i2}U_{j2}$	✗		✗			
	$(Re(a_H)-Re(a'_H))\,U_{i2}U_{j1}$	✓		✓			
	$(Re(a_H)-Re(a'_H))\,U_{i1}U_{j2}$	✓		✓			
	$(2Re(\lambda'_{SH})-\lambda_{SH})\,U_{i1}U_{j1}$	✗		✗			
$S_i'S_j'h$	$(2\lambda''_{DH}+\lambda_{DH}-\lambda'_{DH})U'_{i2}U'_{j2}$					✗	✗
	$(Re(a_H)+Re(a'_H))\,U'_{i1}U'_{j2}$					✗	✗
	$(Re(a_H)+Re(a'_H))\,U'_{i2}U'_{j1}$					✗	✗
	$(2Re(\lambda'_{SH})+\lambda_{SH})\,U'_{i1}U'_{j1}$					✗	✗
$S_iS_j'h$	$(Im(a'_H)-Im(a_H))\,U_{i2}U'_{j1}$		✗		✗		
	$(Im(a_H)+Im(a'_H))\,U_{i1}U'_{j2}$		✗		✗		
	$Im(\lambda'_{SH})U'_{i1}U'_{j1}$		✗		✗		

Table 3 The couplings in scenario II

	couplings	S_1S_1h	$S_1S_1'h$	S_1S_2h	$S_1S_2'h$	$S_1'S_1'h$	$S_1'S_2'h$
S_iS_jh	$(2\lambda''_{DH}-\lambda_{DH}+\lambda'_{DH})U_{i2}U_{j2}$	✗		✗			
	$(Re(a_H)-Re(a'_H))\,U_{i2}U_{j1}$	✗		✗			
	$(Re(a_H)-Re(a'_H))\,U_{i1}U_{j2}$	✗		✗			
	$(2Re(\lambda'_{SH})-\lambda_{SH})\,U_{i1}U_{j1}$	✗		✗			
$S_i'S_j'h$	$(2\lambda''_{DH}+\lambda_{DH}-\lambda'_{DH})U'_{i2}U'_{j2}$					✗	✗
	$(Re(a_H)+Re(a'_H))\,U'_{i1}U'_{j2}$					✓	✓
	$(Re(a_H)+Re(a'_H))\,U'_{i2}U'_{j1}$					✓	✓
	$(2Re(\lambda'_{SH})+\lambda_{SH})\,U'_{i1}U'_{j1}$					✗	✗
$S_iS_j'h$	$(Im(a'_H)-Im(a_H))\,U_{i2}U'_{j1}$		✗		✗		
	$(Im(a_H)+Im(a'_H))\,U_{i1}U'_{j2}$		✗		✗		
	$Im(\lambda'_{SH})U'_{i1}U'_{j1}$		✗		✗		

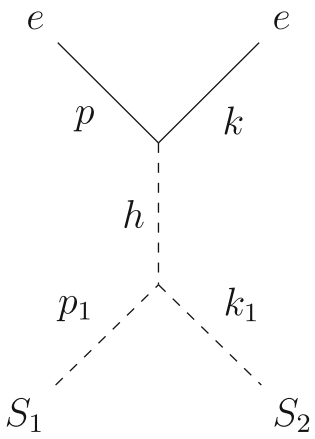

Fig. 4 The Higgs mediated DM-electron scattering

4.3 Scenario III: Higgs mediated $\mathbb{S}_1 N \to \mathbb{S}_2 N'$

Since the couplings a_H, a'_H, and λ'_{SH} can be complex numbers, the CP-violation interactions with Higgs field arise. In this scenario, we employ four-dimensional mass matrix as shown in Eq. 21, and the mass eigenstates are denoted by $\mathbb{S}_i$. Therefore, we have $\mathbb{S}_1\mathbb{S}_2 h$ interaction as presented in Fig. 3c, which shows the coupling between that Higgs field, CP-even and CP-odd parts of scalar fields.

In Table 4, the green marks mean that the $\mathbb{S}_1\mathbb{S}_4 h$ and $\mathbb{S}_2\mathbb{S}_4 h$ interactions are suppressed by the mass splittings between $\mathbb{S}_1$ and $\mathbb{S}_4$, as well as $\mathbb{S}_2$ and $\mathbb{S}_4$, respectively. The benchmark point is Point 3 in Table 5.

4.4 Scenario IV: Z mediated $S_1 N \to S'_1 N'$

As shown in Fig. 3d, because there exists the mass splitting between the real and imaginary parts of scalar fields, we have the Z mediated DM-nucleon inelastic scattering. The $S_1 S'_1 Z$ interaction will be large when the mass difference between S_1 and S'_1 is small, and the mixings in both real and imaginary parts are large. The corresponding benchmark point is Point 4 in Table 5, where we rescaled the cross section of DM direct direction by $\sigma_{SI}^{\text{Rescaled}} = \sigma_{SI} \cdot \Omega_{\text{DM}}/0.12$.

5 The XENONNT experimental constraints

The XENON1T experiment announced the low-energy electronic recoil events below 7 keV, which was excluded by the XENONnT experiment. Such latest result sets new limits on numerous new physics models. We will investigate the DM-electron inelastic scattering processes mediated by Higgs and Z bosons, and discuss the constraints on these two processes in light of the XENONnT experiment data. The matrix element of Fig. 4 is

$$i\mathcal{M}_{\text{free}} = \frac{\bar{u}(k)(-i\frac{y_e}{\sqrt{2}})u(p)\cdot V_{SSh}}{(k_1-p_1)^2 - M_h^2}, \tag{22}$$

$$\begin{aligned} V_{SSh} = -\frac{i}{2}\Big(& U_{11}\Big(\left(2\lambda_{SH} - 4\lambda'_{SH}\right) v U_{21} \\ & + \sqrt{2}\left(a'_H - a_H\right) U_{22}\Big) \\ & + U_{11}\Big(\left(2\lambda_{DH} - 2\lambda'_{DH} - 4\lambda''_{DH}\right) v U_{22} \\ & + \sqrt{2}\left(a'_H - a_H\right) U_{21}\Big)\Big), \end{aligned} \tag{23}$$

where V_{SSh}, U_{ij}, and y_e are the vertex of $S_1 S_2 h$, mixing matrix of real part of scalars, and Yukawa coupling of electron, respectively. The differential cross section is

$$\begin{aligned} d\sigma = & \frac{1}{2E_p 2E_{p_1}} \frac{d^3\boldsymbol{k}}{(2\pi)^3 2E_k} \frac{d^3\boldsymbol{k_1}}{(2\pi)^3 2E_{k_1}} \\ & \times (2\pi)^4 \delta^4\left(p + p_1 - k - k_1\right) \overline{|\mathcal{M}_{\text{free}}|^2}. \end{aligned} \tag{24}$$

The real case is that DM scatter with electron in a bound state, and thus we should take the wavefunction of initial and final state into account. Such effects can be parameterized as an atomic form factor $f_{ion}^{nl}(q)$.

The differential cross section with the fixed DM velocity (v_S) is [29–31]

$$\frac{d\sigma_{Se}}{dE_R} = \frac{\bar{\sigma}_e}{8E_R v_S^2 \mu_{Se}^2} \int q dq \, |F_{DM}(q)|^2 \sum_{n,l} \left| f_{\text{ion}}^{nl}(k,q) \right|^2, \tag{25}$$

where σ_{Se} is the scattering cross section of DM and a bound electron, E_R is the recoil energy, μ_{Se} is the DM-electron reduced mass, $F_{DM}(q)$ is the DM form factor, $f_{\text{ion}}^{nl}(k,q)$ is the ionization form factor of the (n,l) atomic shell, and $k = \sqrt{2m_e E_R}$ is the outgoing momentum of electron.

Following the convention in Ref. [32], the reference momentum transform is fixed at $q = \alpha m_e$. And then the matrix element square and $\bar{\sigma}_e$ are defined by

$$\overline{|\mathcal{M}_{\text{free}}|^2} = \overline{|\mathcal{M}_{\text{free}}(\alpha m_e)|^2} \times |F_{DM}(q)|^2, \tag{26}$$

$$\bar{\sigma}_e = \frac{\mu_{Se}^2 \overline{|\mathcal{M}_{\text{free}}(\alpha m_e)|^2}}{16\pi m_S^2 m_e^2}. \tag{27}$$

The event rate can be written as

$$\frac{dR}{dE_R} = \epsilon(E_R)\, n_T \int_{E_S^{\min}}^{E_S^{\max}} \frac{d\phi_S}{dE_S} \frac{d\sigma_{Se}}{dE_R}, \tag{28}$$

where $\frac{d\Phi_S}{dE_S}$ is the DM flux in the Galactic halo, $n_T = 4.2 \times 10^{27}$/tonne for Xenon, and $\epsilon(E_R)$ is the detection efficiency.

Table 4 The couplings in scenario III

	couplings	$\mathbb{S}_1\mathbb{S}_1h$	$\mathbb{S}_1\mathbb{S}_2h$	$\mathbb{S}_1\mathbb{S}_3h$	$\mathbb{S}_1\mathbb{S}_4h$	$\mathbb{S}_2\mathbb{S}_2h$	$\mathbb{S}_2\mathbb{S}_4h$
$\mathbb{S}_j\mathbb{S}_kh$	$(2\lambda''_{DH}-\lambda_{DH}+\lambda'_{DH})U_{j2}U_{k2}$	✗	✗	✗	✗	✗	✗
	$(Re(a_H)-Re(a'_H))\,U_{j1}U_{k2}$	✗	✗	✗	✗	✗	✗
	$(Re(a_H)-Re(a'_H))\,U_{j2}U_{k1}$	✗	✗	✗	✗	✗	✗
	$(2Re(\lambda'_{SH})-\lambda_{SH})\,U_{j1}U_{k1}$	✗	✗	✗	✗	✗	✗
	$(2\lambda''_{DH}+\lambda_{DH}-\lambda'_{DH})U_{j4}U_{k4}$	✗	✗	✗	✗	✗	✗
	$(2Re(\lambda'_{SH})+\lambda_{SH})\,U_{j3}U_{k3}$	✗	✗	✗	✗	✗	✗
	$(Re(a_H)+Re(a'_H))\,U_{j3}U_{k4}$	✗	✓	✗	✗	✓	✗
	$(Re(a_H)+Re(a'_H))\,U_{j4}U_{k3}$	✗	✓	✗	✗	✓	✗
	$(Im(a'_H)-Im(a_H))\,U_{j3}U_{k2}$	✗	✓	✗	✗	✓	✗
	$(Im(a'_H)-Im(a_H))\,U_{j2}U_{k3}$	✗	✓	✗	✗	✓	✗
	$(Im(a_H)+Im(a'_H))\,U_{j4}U_{k1}$	✗	✓	✗	✗	✗	✗
	$(Im(a_H)+Im(a'_H))\,U_{j1}U_{k4}$	✓	✓	✗	✗	✗	✗
	$Im(\lambda'_{SH})U_{j3}U_{k1}$	✓	✓	✗	✗	✗	✗
	$Im(\lambda'_{SH})U_{j1}U_{k3}$	✓	✓	✗	✗	✗	✗

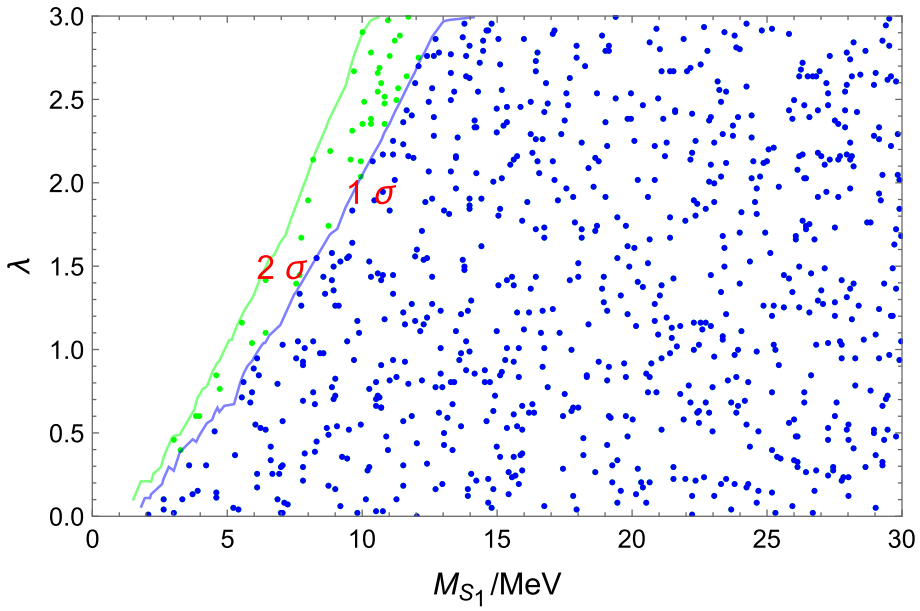

Fig. 5 The constraint on the DM-electron scattering process mediated by Higgs particle

In Fig. 5, we redefine an effective coupling $\lambda = V_{SSh}/v$ for the small mixing of singlet and doublet scalars. A conservative range $\lambda \leq 3$ is employed to avoid large quantum corrections, and the mass difference between S_1 and S_2 is fixed at about 2.5 keV. We present the viable parameter space in the λ vs M_{S_1} plane for the DM-electron scattering process mediated by Higgs particle which are consistent with the XENONnT data within 1 σ (blue dots) region and 2 σ region (blue and green dots). And the DM mass around several MeVs can be excluded (blank region).

In addition, with the small mass splitting between the lightest real and imaginary components of the new scalar fields, we can have the inelastic scatting process mediated by the Z boson, as given in Fig. 6. The corresponding matrix element can be written as

$$iM_{\text{free}} = \frac{\bar{u}(k)\left(\frac{1}{2}i\left(g_2\cos\theta_W - g_1\sin\theta_W\right)\left(\gamma^\mu\cdot\frac{1-\gamma_5}{2}\right) - ig_1\sin\theta_W\left(\gamma^\mu\cdot\frac{1+\gamma^5}{2}\right)u(p)\right)\cdot V_{SSZ}}{(k_1-p_1)^2 - M_Z^2}, \tag{29}$$

Table 5 The benchmark points for inelastic DM. All the points are consistent with R_K, $B_s - \bar{B}_s$, muon g-2, Xenon1T direct detection, and DM relic density simultaneously

	Point 1	Point 2	Point 3	Point 4
Relic density	0.120245	0.120063	0.121847	0.00273
M_{S_1}/GeV	62.5280891	63	63.7565163	45.2614126
M_{S_2}/GeV	64.5715733	101.106889	145.249	104.765951
$M_{S'_1}$/GeV	63.3955834	62.8787699	64.0200287	45.2712507
$M_{S'_2}$/GeV	101.106889	64.6181886	145.347221	104.766473
Re(a_H)/GeV	0.138149275	0.161219197	2	16
Re(a'_H)/GeV	− 0.138149275	0.161219197	2	0
Im(a_H)/GeV	0	0	0.0334546373	0
Im(a'_H)/GeV	0	0	0.0503546759	0
M_S/GeV	63	63	64	55
M'_S/GeV	5	0	3.87583889	0.5
M_D/GeV	64.5	64.5	145.249	100
$M_{L'}$/GeV	923.760249	890.911643	902.487	902.908781
$M_{Q'}$/GeV	3935.5024	3937.63785	3933.748	3901.27893
λ_{SH}	0	0	0	0
Re(λ'_{SH})	0	0	0	0
Im(λ'_{SH})	0	0	0.000106455208	0
λ_{DH}	0.2	0.2	0	0
λ'_{DH}	0.1	0.1	0	0
λ''_{DH}	0.05	− 0.05	0	0
λ_2^Q	− 0.31671602	− 0.5704031	− 0.822821	− 0.517382525
λ_3^Q	0.880289647	0.68180215	0.417204	0.555727792
λ_2^L	2.8761966	2.46163782	2.16895	2.76669117
λ_2^E	0.003504851	0.00252737	0.00534	0.001891458
$\lambda_S/2$	− 0.181683181	− 0.339379484	0.36714921	0.042653427
$\lambda'_S/2$	0.897108085	− 0.71839593	− 0.37282701	− 0.661534232
$\lambda''_S/2$	− 0.327292676	0.340974767	− 0.467026357	− 0.055752432
$\lambda_D/2$	− 0.508257921	0.649093836	− 0.656446092	0.853623195
λ_{SD}	0.032597077	0.806907755	0.474364027	0.852904036
λ'_{SD}	− 0.461554286	− 0.192091407	0.68062965	0.825947186
$\sigma_{SI}^{\text{Rescaled}}/\text{cm}^2$	1.139×10^{-49}	2.97×10^{-49}	2.4×10^{-50}	4.68×10^{-47}

$$V_{SSZ} = -\frac{1}{2} U_{12} U'_{12} \left(g_2 \cos\theta_W + g_1 \sin\theta_W\right)(p_1 - k_1)\,, \tag{30}$$

where V_{SSZ}, U_{12}, and U'_{12} are the vertex of $S_1 S'_1 Z$, the mixing matrix element of real, and imaginary parts of scalars, respectively. Also, θ_W is the Weinberg angle, and g_1 and g_2 are the gauge couplings of $U(1)_Y$ and $SU(2)_L$.

We find that the XENONnT data cannot give a constraint on the Z mediated DM-electron scattering process since Z boson is heavy enough and the coupling of $S_1 S'_1 Z$ is suppressed by mixing angles in both real (U_{12}) and imaginary parts (U'_{12}) of scalars.

6 Conclusion

We considered the general scalar potential with CP-violation and the inelastic dark matter in the Simple Extension of the Standard Model (SESM), which can explain the dark matter as well as new physics anomalies such as the B physics anomalies and muon anomalous magnetic moment, etc. With the a_H, a'_H M'^2_S, λ'_{SH}, and λ''_{DH} terms, we obtained the mass splittings for the real and imaginary parts of scalar fields. In particular, we can have the DM co-annihilation process mediated by Z boson, which couples exclusively to the CP-even and CP-odd parts of scalar fields. For the CP conserving case, we presented the viable parameter space for the DM co-annihilation processes through both Higgs and Z reso-

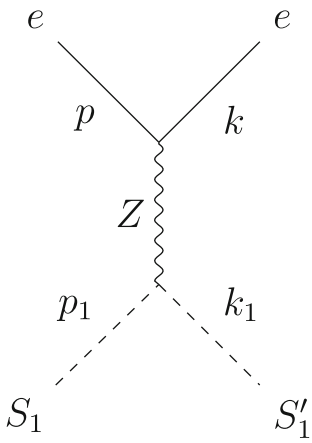

Fig. 6 The Z mediated DM-electron scattering process

nances, which can address the B physics anomalies, muon g-2, and DM relic density, as well as evade the constraint from the XENON1T direct detection simultaneously. For the CP-violating case, we discussed four scenarios for the inelastic DM-nucleon scatterings mediated by the Higgs and Z bosons in details, and presented the benchmark points which satisfy the aforementioned constraints. Finally, with the XENONnT results, we studied the inelastic scattering processes between the DM and electron mediated by Higgs and Z bosons, and found that the constraint on the Z mediated process is weak, while the Higgs mediated process excludes the dark matter with mass around several MeV.

Acknowledgements We are indebted to Lorenzo Calibbi, Jibo He, Junle Pei, and Bin Zhu for the helpful discussions. This research is supported in part by the National Key Research and Development Program of China Grant No. 2020YFC2201504, by the Projects No. 11875062, No. 11947302, No. 12047503, and No. 12275333 supported by the National Natural Science Foundation of China, by the Key Research Program of the Chinese Academy of Sciences, Grant No. XDPB15, by the Scientific Instrument Developing Project of the Chinese Academy of Sciences, Grant No. YJKYYQ20190049, and by the International Partnership Program of Chinese Academy of Sciences for Grand Challenges, Grant No. 112311KYSB20210012.

Data Availability Statement This manuscript has no associated data or the data will not be deposited. [Authors' comment: This is a theoretical study and no experimental data.]

Funded by SCOAP[3]. SCOAP[3] supports the goals of the International Year of Basic Sciences for Sustainable Development.

Appendix A: the relevant vertices

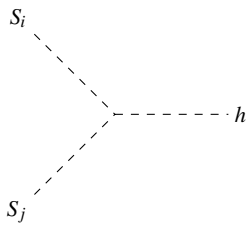

$$\begin{aligned}&\frac{i}{4}\left(4v(2\lambda''_{DH}-\lambda_{DH}+\lambda'_{DH})U_{i2}U_{j2}\right.\\&+2\sqrt{2}\left(Re(a_H)-Re(a'_H)\right)U_{i2}U_{j1}\\&+4v\left(2Re(\lambda'_{SH})-\lambda_{SH}\right)U_{i1}U_{j1}\\&\left.+2\sqrt{2}\left(Re(a_H)-Re(a'_H)\right)U_{i1}U_{j2}\right),\end{aligned}\tag{A1}$$

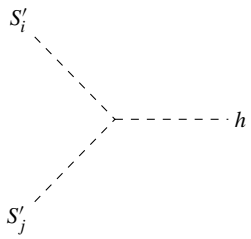

$$\begin{aligned}&-\frac{i}{4}\left(4v\left(2Re(\lambda'_{SH})+\lambda_{SH}\right)U'_{i1}U'_{j1}\right.\\&+2\sqrt{2}\left(Re(a_H)+Re(a'_H)\right)U'_{i1}U'_{j2}\\&+4v\left(2\lambda''_{DH}-\lambda'_{DH}+\lambda_{DH}\right)U'_{i2}U'_{j2}\\&\left.+2\sqrt{2}\left(Re(a_H)+Re(a'_H)\right)U'_{i2}U'_{j1}\right),\end{aligned}\tag{A2}$$

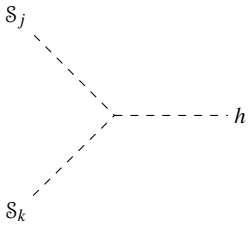

$$
\begin{aligned}
&\frac{i}{4}\Big(-8vU_{j3}U_{k1}Im(\lambda'_{SH}) \\
&-2\sqrt{2}U_{j4}U_{k1}\left(Im(a_H)+Im(a'_H)\right) \\
&+2\sqrt{2}U_{j3}U_{k2}\left(Im(a'_H)-Im(a_H)\right) \\
&-4vU_{j3}U_{k3}\left(2Re(\lambda'_{SH})+\lambda_{SH}\right) \\
&-2\sqrt{2}U_{j4}U_{k3}\left(Re(a_H)+Re(a'_H)\right) \\
&+4vU_{j2}U_{k2}\left(2\lambda''_{DH}-\lambda_{DH}+\lambda'_{DH}\right) \\
&+2\sqrt{2}U_{j2}U_{k1}\left(Re(a_H)-Re(a'_H)\right) \\
&+2\sqrt{2}U_{j2}U_{k3}\left(Im(a'_H)-Im(a_H)\right) \\
&-2\sqrt{2}U_{j3}U_{k4}\left(Re(a_H)+Re(a'_H)\right) \\
&+4vU_{j4}U_{k4}\left(\lambda'_{DH}-2\lambda''_{DH}-\lambda_{DH}\right) \\
&-4vU_{j1}U_{k1}\left(\lambda_{SH}-2Re(\lambda'_{SH})\right) \\
&+2\sqrt{2}U_{j1}U_{k2}\left(Re(a_H)-Re(a'_H)\right) \\
&-\ 8vU_{j1}U_{k3}Im(\lambda'_{SH}) \\
&-2\sqrt{2}U_{j1}U_{k4}\left(Im(a_H)+Im(a'_H)\right)\Big)
\end{aligned}
\tag{A3}
$$

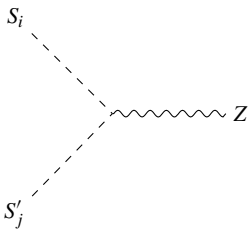

$$
-\frac{1}{2}\left(g_1\sin\theta_W+g_2\cos\theta_W\right)U_{i2}U'_{j2}\left(-p_\mu^{S'_j}+p_\mu^{S_i}\right). \tag{A4}
$$

References

1. G. Aad et al. [ATLAS], Phys. Lett. B **716**, 1–29 (2012). arXiv:1207.7214 [hep-ex]
2. S. Chatrchyan et al. [CMS], Phys. Lett. B **716**, 30–61 (2012). arXiv:1207.7235 [hep-ex]
3. R. Aaij et al. [LHCb], Nat. Phys. **18**(3), 277–282 (2022). arXiv:2103.11769 [hep-ex]
4. W. Altmannshofer, P. Stangl, Eur. Phys. J. C **81**(10), 952 (2021). arXiv:2103.13370 [hep-ph]
5. J. Aebischer, W. Altmannshofer, D. Guadagnoli, M. Reboud, P. Stangl, D.M. Straub, Eur. Phys. J. C **80**(3), 252 (2020). arXiv:1903.10434 [hep-ph]
6. J. Albrecht, S. Reichert, D. van Dyk, Int. J. Mod. Phys. A **33**(18n19), 1830016 (2018). arXiv:1806.05010 [hep-ex]
7. Y. Li, C.D. Lü, Sci. Bull. **63**, 267–269 (2018). arXiv:1808.02990 [hep-ph]
8. S. Bifani, S. Descotes-Genon, A. Romero Vidal, M.H. Schune, J. Phys. G **46**(2), 023001 (2019). arXiv:1809.06229 [hep-ex]
9. P. Arnan, L. Hofer, F. Mescia, A. Crivellin, JHEP **04**, 043 (2017). arXiv:1608.07832 [hep-ph]
10. P. Arnan, A. Crivellin, M. Fedele, F. Mescia, JHEP **06**, 118 (2019). arXiv:1904.05890 [hep-ph]
11. W. Yin, M. Yamaguchi, Phys. Rev. D **106**(3), 033007 (2022). arXiv:2012.03928 [hep-ph]
12. [LHCb], arXiv:2212.09152 [hep-ex]
13. [LHCb], arXiv:2212.09153 [hep-ex]
14. B. Abi et al. [Muon g-2], Phys. Rev. Lett. **126**(14), 141801 (2021). arXiv:2104.03281 [hep-ex]
15. M. Lindner, M. Platscher, F.S. Queiroz, Phys. Rep. **731**, 1–82 (2018). arXiv:1610.06587 [hep-ph]
16. R. Capdevilla, D. Curtin, Y. Kahn, G. Krnjaic, Phys. Rev. D **103**(7), 075028 (2021). arXiv:2006.16277 [hep-ph]
17. D. Buttazzo, P. Paradisi, Phys. Rev. D **104**(7), 075021 (2021). arXiv:2012.02769 [hep-ph]
18. R. Capdevilla, D. Curtin, Y. Kahn, G. Krnjaic, Phys. Rev. D **105**(1), 015028 (2022). arXiv:2101.10334 [hep-ph]
19. T. Li, J. Pei, W. Zhang, Eur. Phys. J. C **81**(7), 671 (2021). arXiv:2104.03334 [hep-ph]
20. W. Ahmed, I. Khan, J. Li, T. Li, S. Raza, W. Zhang, Phys. Lett. B **827**, 136879 (2022). arXiv:2104.03491 [hep-ph]
21. B. Zhu, X. Liu, Sci. China Phys. Mech. Astron. **65**(3), 231011 (2022). arXiv:2104.03238 [hep-ph]
22. L. Calibbi, M.L. López-Ibáñez, A. Melis, O. Vives, Eur. Phys. J. C **81**(10), 929 (2021). arXiv:2104.03296 [hep-ph]
23. G. Arcadi, L. Calibbi, M. Fedele, F. Mescia, Phys. Rev. Lett. **127**(6), 061802 (2021). arXiv:2104.03228 [hep-ph]
24. G. Bertone, D. Hooper, J. Silk, Phys. Rep. **405**, 279–390 (2005). arXiv:hep-ph/0404175 [hep-ph]
25. E. Aprile et al. [XENON], Phys. Rev. D **102**(7), 072004 (2020). arXiv:2006.09721 [hep-ex]
26. E. Aprile, K. Abe, F. Agostini, S.A. Maouloud, L. Althueser, B. Andrieu, E. Angelino, J.R. Angevaare, V.C. Antochi, D.A. Martin et al., arXiv:2207.11330 [hep-ex]
27. L. Calibbi, T. Li, Y. Li, B. Zhu, JHEP **10**, 070 (2020). arXiv:1912.02676 [hep-ph]
28. T. Li, J. Pei, X. Yin, B. Zhu, arXiv:2205.08215 [hep-ph]
29. Q.H. Cao, R. Ding, Q.F. Xiang, Chin. Phys. C **45**(4), 045002 (2021). arXiv:2006.12767 [hep-ph]
30. L. Su, W. Wang, L. Wu, J.M. Yang, B. Zhu, Phys. Rev. D **102**(11), 115028 (2020). arXiv:2006.11837 [hep-ph]
31. S.M. Choi, H.M. Lee, B. Zhu, JHEP **04**, 251 (2021). arXiv:2012.03713 [hep-ph]
32. R. Essig, J. Mardon, T. Volansky, Phys. Rev. D **85**, 076007 (2012). arXiv:1108.5383 [hep-ph]
33. L. Di Luzio, M. Kirk, A. Lenz, T. Rauh, JHEP **12**, 009 (2019). arXiv:1909.11087 [hep-ph]
34. L. Silvestrini, M. Valli, Phys. Lett. B **799**, 135062 (2019). arXiv:1812.10913 [hep-ph]